Magnetic Field Triggered Switching of High-Temperature Superconductors—Basic Experiments

Quoc Hung Pham, Mathias Noe, and Andrej Kudymow

***Abstract*—High-temperature superconductors have a wide range of applications due to their high availability and excellent performance. One attractive technology is using superconductors as switches. In general, a change of resistance can be achieved by temperature, current, or magnetic field. In the latter case, a dynamic resistance can be obtained by an alternating magnetic field and has been investigated in this work. These properties enable zero ON-state resistance and fast switching times. The magnetic field has been generated by an iron magnet with an air gap of 1 mm and penetrated the superconductor perpendicular to the ab-plane. The dynamic resistance of one superconducting high-temperature superconductor (HTS) tape has been measured for magnetic flux densities up to 340 mT and frequencies up to 500 Hz in liquid nitrogen at 77 K. The experimental results have been compared with simulation models. In addition, a parallel circuit of two superconducting switching units was set up where each magnet was controlled individually and switched in an alternating mode. The commutation time, dependent on the magnetic field's amplitude and frequency, was measured. With this setup, a resistance of 13.14 mΩm^{-1} has been achieved. Commutation times below 5 ms could be achieved with rare-earth barium copper oxide tapes.**

***Index Terms*—Dynamic resistance, coated conductor, high-temperature superconductor (HTS), rare-earth barium copper oxide.**

I. Introduction

IT IS well known that the superconducting state of superconductors depends on the temperature, the current, and the magnetic field. The transition to the normal conducting state, the so-called quench, takes place when only one of the critical parameters is exceeded. For each parameter applications already exist, that use the quench that is either triggered by the temperature, the current, or the magnetic field.

Magnets with superconducting contacts use, for example, heaters to ramp up the magnet and run the magnet afterward in persistent mode. This transition is relatively slow and takes place usually in several seconds up to minutes [1], [2], [3]. Nearly instantaneous, the quench is used in resistive fault current limiters to limit the short-circuit current, when the critical current of the superconductors is exceeded [4], [5], [6]. Furthermore, it has been shown, that a very fast triggering of superconductors with a magnetic field can be used in a flux pump [7], [8], [9], [10], [11], [12], [13], [14]. In [10], a flux pump with two switches is shown but not the interaction between these switches.

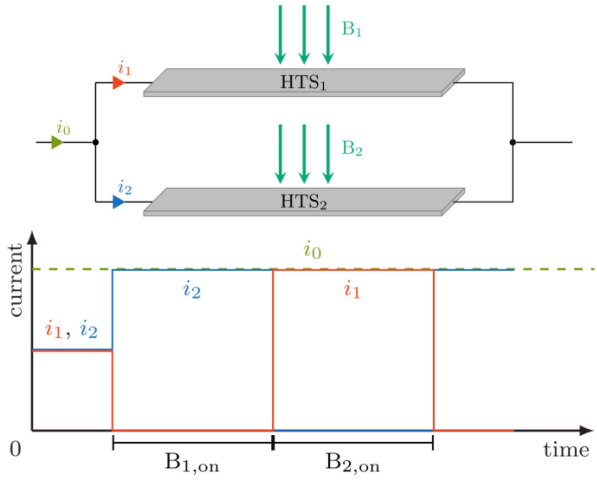

Fig. 1. Schematic drawing of the experimental setup with two superconductors in parallel. Below is the ideal current distribution achieved by triggering the alternating magnetic field.

In this article, basic experiments are presented with a fast triggering of superconductors with magnetic fields that develop a dynamic resistance. The general setup of the main experiments is shown in Fig. 1 with its function and basic current behavior.

Two high-temperature superconductors are connected in parallel, and a varying magnetic field is applied as shown in Fig. 1. The focus of this article is to experimentally investigate the interaction between these switches and the commutation behavior of the currents while triggering the superconductors with magnetic fields that vary in magnitude and frequency. First, experiments are carried out on one superconducting switch measuring the dynamic resistance. Then, the combination of two switches is investigated. The experimental results are confirmed by analytical equations and possible applications are discussed.

II. Experimental Setup

The following experimental setup has been used to show basic current switching between two parallel superconducting paths and is shown in Fig. 2.

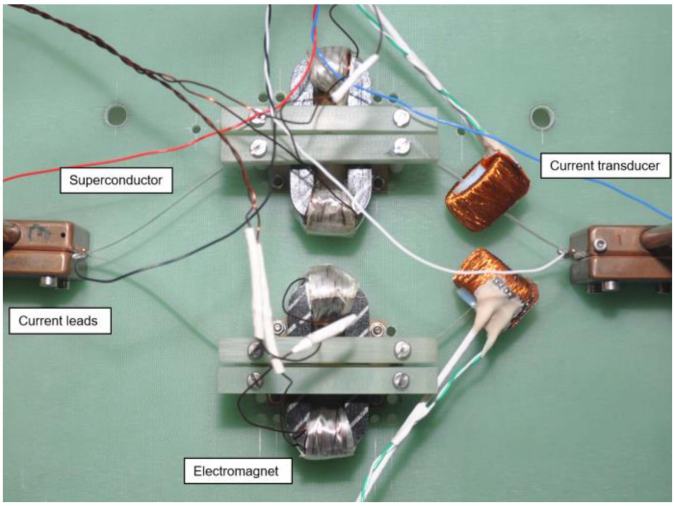

Fig. 2. Experimental setup with a sliced superconductor.

A. Setup

The two superconductors were connected at both ends with copper current leads. The magnetic field is applied to each superconductor by electromagnets which can be switched ON and OFF independently of each other. The electromagnet consists of two U-shaped laminated iron cores. Each core has a 50-turn winding of Cu magnet wire with a diameter of 0.75 mm. The total active length with a magnetic field affecting the superconductor is 2 cm. To place the superconductor in the magnet, a 1 mm wide air gap was created between the two iron cores with spacers. The magnetic flux density in the air gap B_{airgap} was measured as a function of the dc coil current I_{coil} with a hall probe of the type HHP-VP manufactured by AREPOC. For a dc coil current of 20 A, a homogeneous maximum magnetic field of 1.2 T was achieved.

To be able to neglect the influence of different joint resistances of the two superconducting paths, a 23 cm long slot has been laser cut into a 12 mm wide tape with a total length of 35 cm. Since both superconducting paths were made from just one superconductor, it can be assumed that there is no contact resistance between the two parallel paths, and both are equally connected to the current source. The ends of the superconductor are clamped into the current leads over a length of 5 cm. A thin indium foil is used to reduce contact resistance and damage due to mechanical stress.

A current sensing system based on a closed-loop compensated hall sensor was made to measure the current in each superconductor [15], [16]. This method can be used to measure dc and transient currents contactless. Those current transducers use a ferromagnetic core with a magnetic field sensor inserted in an air gap of the core. The core picks up the magnetic flux density of the primary winding and the changes in a magnetic field are measured. This field is compensated with the secondary winding on the iron core, which creates an opposing magnetic field. The current that is needed can be measured with a shunt resistor and is directly proportional to the current flowing in the primary winding. The iron core used has an outer diameter of 30 mm with a thickness of 3 mm and is shown in Fig. 2 on the right side and is equipped with a secondary winding with approx. 2500 turns. Due to the operation in liquid nitrogen, the core, and the electronics were separated.

A dc power supply (Keysight RP7943A) was used to feed dc current to the superconductor. For energizing the electromagnets two bipolar power supplies (Kepco BOP 72-6) were controlled by a four-channel arbitrary waveform generator (Tabor WW5064).

For measuring the critical current of the sample two voltages were measured. The first voltage taps are placed with a distance of 23 cm within the current flowing area and the second outside the current leads at a distance of 33 cm. The output voltages of the voltage taps were measured using a multiplexer (HP 34970A) with an external dc nanovolt-meter (HP 34420A). For capturing transients, a digital oscilloscope (Keysight InfiniiVision DSOX3024A was used.

TABLE I
REBCO CONDUCTOR SPECIFICATIONS

Manufacturer	SuperPower
Model	SF12100
Self-field critical current at 77 K	380 A
Sample width	12 mm
Thickness of Ag stabilizer layer each side	1.0 μm
Thickness of superconductor layer	1.0 μm
Thickness of substrate	100 μm
Resistance per length at RT	3.175 m$\Omega\cdot$cm^{-1}
Resistance per length* at 77 K	0.729 m$\Omega\cdot$cm^{-1}
Critical temperature	92 K

Note: *resistance of tape at 77 K with superconducting layer at normal conducting conditions.

B. Superconductor

For the following experiments, a noncopper stabilized second-generation high-temperature superconductor was selected. The 12 mm wide tape is fabricated by SuperPower (SF12100) and has a self-field critical current I_c of 380 A at 77 K. The tape mainly consists of a thin 1 μm thin film of superconducting rare-earth barium copper oxide (ReBCO) and a metal tape for mechanical stabilization. In between, several buffer layers adjust the lattice of both materials. This is then surrounded by a thin silver layer which functions as a chemical barrier and partly as electrical stabilization in case of a quench. The key specifications of the sample are shown in Table I. The thicknesses of the layers were measured by scanning electron microscope image processing and the resistances were measured with four-terminal sensing. To measure the resistance of the normal conducting layers at 77 K the superconducting layer has been disabled by heating with dc current.

C. Dynamic Resistance

The basic principle of ac field switches is based on the dynamic resistance that occurs when a dc current-carrying superconductor experiences an external perpendicular alternating

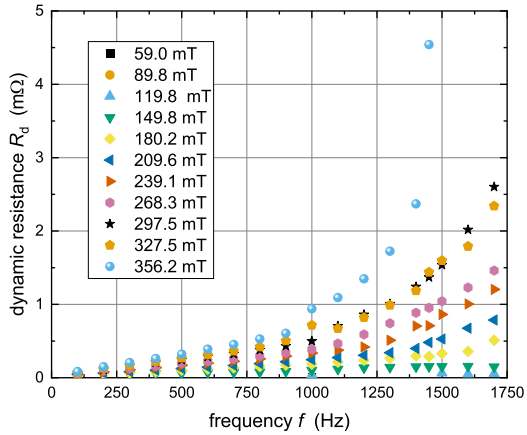

Fig. 3. Measured dynamic resistance for various frequencies and amplitudes of applied external alternating magnetic field.

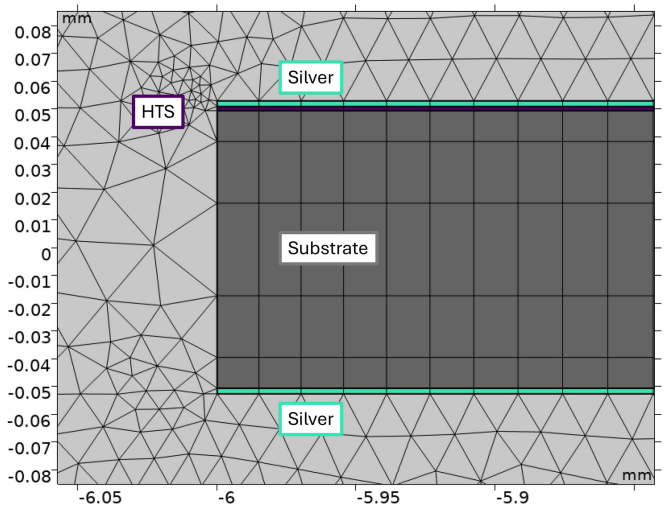

Fig. 4. Section of the modelled geometry in COMSOL with the fully modelled HTS tape and the surrounding air. In the tape has a mapped mesh and the air a triangular.

magnetic field [17], [18]. In this state, losses due to flux movements inside the superconducting material are produced which results in a voltage drop along the length of the superconductor proportional to the current. This phenomenon was further investigated by Jiang et al. [19] resulting in the following equation for the dynamic resistance $R_{d,\perp}$:

$$R_{d,\perp} = \frac{4afL}{I_{c0}} \left(B_{a,\perp} - B_{\text{th},\perp}\right) \tag{1}$$

where L is the length of the superconductor which an external field is applied on, a is the half width of the slab, f is the frequency of the magnetic field, I_{c0} is the critical current, $B_{a,\perp}$ is the amplitude of the applied perpendicular field, and $B_{\text{th},\perp}$ is the threshold field defined by

$$B_{\text{th},\perp} = \frac{4.9284\mu_0 J_{c0} t}{\pi} \left(1 - i\right) \tag{2}$$

with $J_{c0} = I_{c0}\ /4at$ where $2t$ is the thickness of the superconducting layer, and $i\ = I_t\ /I_{c0}$ with the transport dc current I_t. The threshold field $B_{\text{th},\perp}$ is the maximal field amplitude for which the superconductor can shield the external field from penetrating the central region.

Equation (1) shows that the dynamic resistance is a function of the frequency and the amplitude of the applied magnetic field. Therefore, high field and high frequency are required to build up a high dynamic resistance.

III. Basic Experiments

A. Measurement of the Dynamic Resistance

The dynamic resistance as a function of the frequency and amplitude of the magnetic field is shown in Fig. 3. The dynamic resistance is measured by the voltage drop over 2 cm of the superconductor subjected to an external magnetic field while applying a dc current to the superconductor. In this setup, the parallel superconductor is replaced by 12 mm x 250 μm copper tape to provide an alternative current path in case of a quench. The dc current is increased in 0.5 A steps to 20 A.

For low frequencies, the dynamic resistance increases linearly with the frequency and agrees with the analytic equation (1). With higher frequencies and amplitudes of the magnetic field, a nonlinear increase can be observed and reaches up to 4.5 mΩ for 1450 Hz and 356.17 mT. So, two effects can be seen. For fixed magnetic amplitude the dynamic resistance increases linearly at first and transitions into a nonlinear behavior for higher frequencies. This phenomenon is already shown and discussed in several previous works [20], [21], [22], [23], [24]. The transport current distribution is highly dependent on the frequency, shifting the current initially flowing in the superconducting layer to the normal conducting layers which have a resistance and therefore contributes more to the losses with rising frequency. It is also noticeable that with fixed frequency the resistance increases in a nonlinear way with the magnetic field. This phenomenon is already known and shown in [18], [19], [25], and [26]. In [25], Zhang et al. stated that the nonlinear rise occurs when the real load ratio $I_t/I_c(B)$ is reaching 1 resulting in additional flux flow resistance. Additionally, the temperature of the superconducting tape rises due to high losses resulting in lower superconductor performance [27].

The measured dynamic resistances at 500 Hz and different amplitudes were examined in more detail and compared with (1) and a numerical electromagnetic model of the superconductor. A simple numerical model was implemented based on the H-formulation based on paper [26] using COMSOL. A section of the model geometry is displayed in Fig. 4. The individual domains of the high-temperature superconductor (HTS) tape are color-coded.

The model also includes the nonsuperconducting layers apart from the buffer layer, namely the top silver cap, the superconducting layer, the substrate, and the bottom silver cap. The surrounding silver is simplified to a top and a bottom layer. The temperature is constant at 77 K, so no temperature dependence is considered. The superconducting tape is modeled according to the geometric dimensions in Table I. The surrounding air domain is circular and has the diameter of ten times the largest tape dimension. The resistivity is 1.228 $\mu\Omega$m for the substrate,

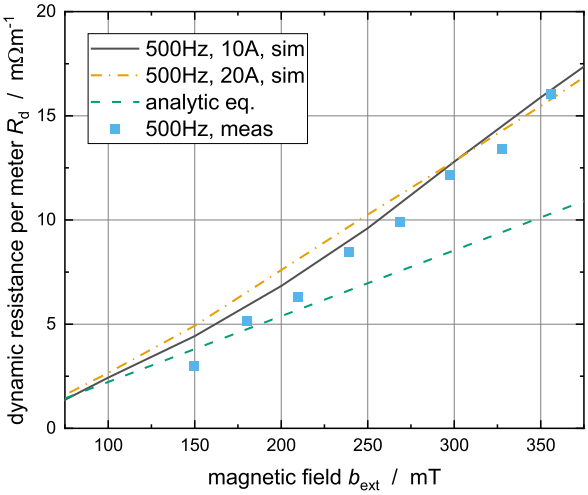

Fig. 5. Measured dynamic resistance per length at 500 Hz and different magnetic field amplitudes compared to analytical equation and numerical simulations.

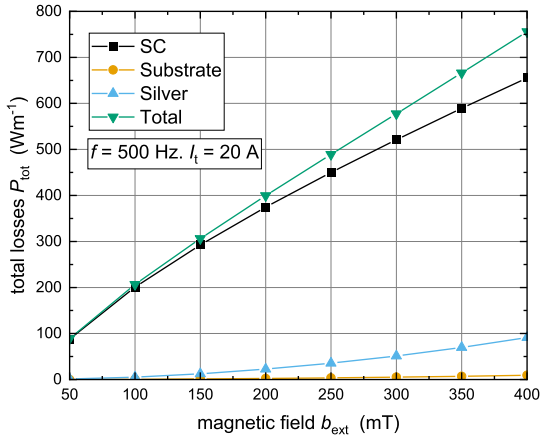

Fig. 6. Losses in the individual layers of a superconducting tape in an external field with transport current.

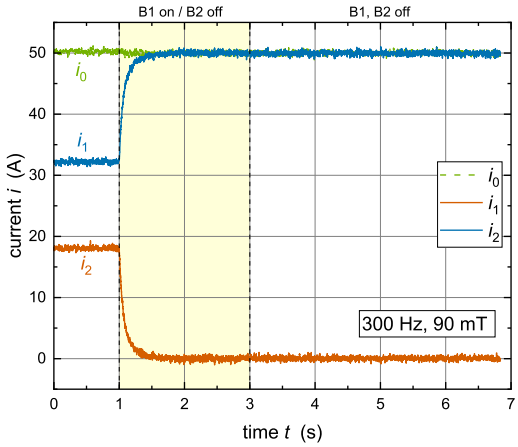

Fig. 7. Current distribution of single-sided triggering.

2.5 nΩm for silver and 2 Ωm for the air domain. Since no magnetic field angle-dependent critical current measurements for this superconducting tape are available, an angular dependent model in elliptical form [28], [29] has been chosen with parameters from works [20] and [21]. The parameters are $k = 0.29515$, $B_0 = 0.04265$ T and $\alpha = 0.7$. The critical current at self-field is taken from the measurement of the real tape as listed in Table I. The mesh of the superconducting tape is mapped with 400 elements along the width. To get a higher resolution at the edges of the tape, the size of each element is increased toward the center.

The results are displayed in Fig. 5 where the dynamic resistance is normalized to the length of the active magnetic field. The measured values are represented as points and show a linear trend depending on the magnetic field and reach up to 16 mΩm^{-1}. The gradient is in good agreement with the numerical simulations. The absolute values are in the same range but differ slightly. The measured values are between the lower analytical values and the higher numerical values. Also, the difference between both numerical calculations for 10 and 20 A transport current is small. The nonlinear rise is noticeable for the measurement and numerical calculations. At around 300 mT, the dynamic resistance at $I_t = 10$ A is greater than that of 20 A. This phenomenon needs to be investigated further elsewhere.

The total losses of the superconducting tape split into each layer are displayed in Fig. 6 for a frequency of 500 Hz and transport current of 20 A depending on the external magnetic field. The total losses per meter are reaching from 87.3 Wm^{-1} at 50 mT to 653.8 Wm^{-1} at 400 mT. For small magnetic fields, losses mainly occur in the superconducting layer. With a higher field, the losses in the normally conducting layers, especially in the silver, are added. Due to the high losses, an increase in temperature in the superconductor is to be expected, despite the bath cooling. A more advanced multiphysics model as in [27], [30], and [31] is needed to predict the temperature and the influence on the superconductor parameters. These models include the general heat transfer equation with a constant heat transfer coefficient of 800 W m^{-2}K^{-1}, but [32] and [33] show that the heat flux is highly dependent on the temperature difference from superconducting to surrounding fluid and the surface roughness of the tape. The heat flux is spread over several magnitudes of order. Therefore, a constant heat transfer coefficient is insufficient to accurately calculate the temperature dependent dynamic losses. A more sophisticated approach which is not within the scope of this work is needed.

B. *Single-Sided Triggering*

At first, the switching behavior of one superconductor was analyzed. For this, a dc transport current I_t of 50 A was applied to the superconductor, and only magnet B1 is switched ON and OFF. The results of this experiment are shown in Fig. 7 which displays the current of both superconducting legs and the sum of currents resulting in a total current of 50 A. With all magnets OFF, the current distribution is 18 A on the first superconductor and 32 A on the second. Since both superconducting paths are part of one 12 mm wide tape, there is no joint resistance explaining the difference in current. Reasons can be imperfections and inhomogeneities in the superconducting layer or slight differences in the geometry of both superconducting paths, therefore

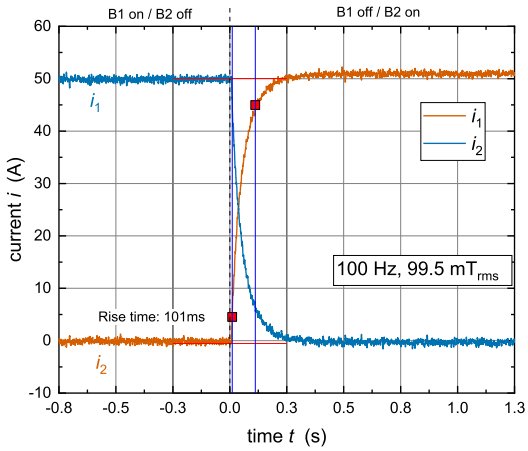

Fig. 8. Current distribution of double-sided triggering. Current fully redistributes to the other parallel superconducting leg.

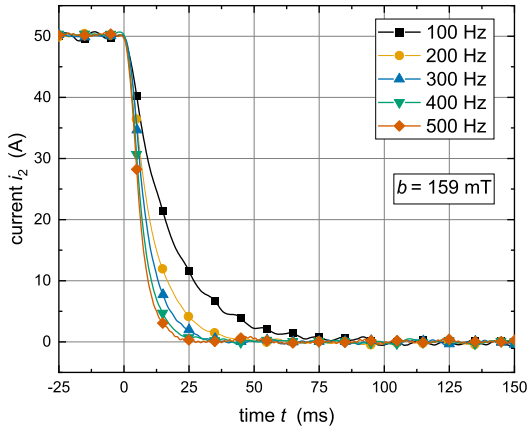

Fig. 9. Course of the current i_2 in the second superconductor when switching magnet 2 on while varying the frequency of the magnetic field.

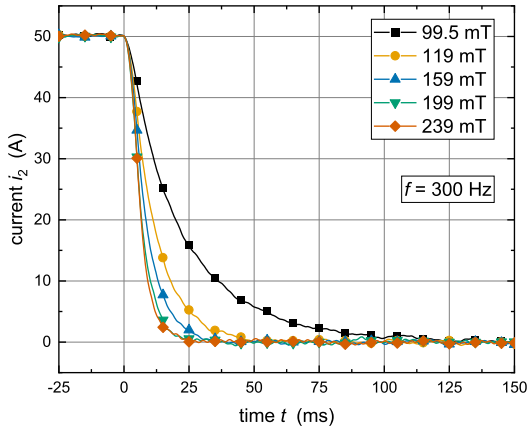

Fig. 10. Course of the current i_2 in the second superconductor when switching magnet 2 on while varying the amplitude of the magnetic field.

slightly different inductances. At time $t = 1$ s, magnet B1 is switched on and creates an alternating magnetic field amplitude of 90 mT with a frequency of 300 Hz. The current redistributes to flow fully in the second superconductor exponentially, rising from 10% to 90% in 210 ms which equals to a time constant $\tau = 95.6$ ms. At $t = 3$ s the magnet is switched OFF and the current distribution remains the same for the rest of the data acquisition time. This behavior shows that there is no joint resistance between both superconducting legs and the critical current of the superconductor has not been exceeded.

IV. Basic Experiments—Double-Sided Triggering

A. Description of the Experiment

The switching behavior with two magnets switching in an alternating pattern is investigated. This means, instead of having equal current distribution in both superconducting legs, the current is flowing only in one superconductor, and at the time of switchover, the current redistributes completely to the other parallel superconducting path. This behavior is shown in Fig. 8 for a magnetic excitation of 100 Hz and 99.5 $\mathrm{mT_{rms}}$. The switchover time is at $t = 0$ s. A total current of 50 A is applied to the parallel circuit of two superconductors. By applying an alternating magnetic field to the first superconducting leg, the current distribution is $i_1 = 0$ A and $i_2 = 50$ A before the switchover time. At $t = 0$ s, magnet B1 is switched OFF and B2 switched ON, resulting in $i_1 = 50$ A and $i_2 = 0$ A. The transitioning is exponential and with a rise time of 101 ms from 10% to 90% or $\tau = 46$ ms. The 10% and 90% points are marked with a red square. The frequency and amplitude of the magnetic field were varied to study the impact on the transition time due to different dynamic resistances.

B. Variation of Frequency f

In Fig. 9, the time-dependent current i_2 in the second superconducting leg is shown for frequencies from 100 to 500 Hz in steps of 100 Hz at a fixed magnetic field amplitude of 159.2 $\mathrm{mT_{rms}}$. The switchover point of the magnets is at $t = 0$ ms. It can be noted that with increasing frequency the falling time of the current decreases from $\tau = 15.7$ ms at 100 Hz to $\tau = 4$ ms at 500 Hz.

C. Variation of Magnetic Field Amplitude $\hat{B}$

Fig. 10 shows the current i_2 before and after the switchover time for different magnetic field amplitudes from 99.5 to 239 mT at a constant frequency of 300 Hz. At first, the transport current of 50 A is flowing completely in the second superconductor. At $t = 0$ ms B1 is switched OFF and B2 on resulting in a redistribution of the current to the first superconductor. With increasing amplitude, the fall time decreases, enabling faster switching times. The measured fall times reach from $\tau = 133.6$ ms to $\tau = 4.2$ ms.

The rise times of all amplitude and frequency combinations are listed in Table II and reach from $\tau = 170.1$ ms at 100 Hz and 59.7 $\mathrm{mT_{rms}}$ to $\tau = 2.5$ ms at 500 Hz and 238.8 $\mathrm{mT_{rms}}$.

The rise time is dependent on the dynamic resistance and the inductivity of the whole circuit. A simplified equivalent circuit is shown in Fig. 11. The inductivity depends on the length and the geometry of the superconductor.

TABLE II
RISE AND FALL TIME FOR DIFFERENT MAGNETIC FIELD AMPLITUDES AND FREQUENCIES FOR DOUBLE-SIDED TRIGGERING

Magnetic Field Amplitude $\hat{b}$ (mT_{rms})	Time constant τ (ms)	Frequency f (Hz) 100	150	200	250	300	350	400	450	500
	59.7	170.1	158.4	149.5	145.6	133.6	123.2	124.2	93.9	91.5
	79.6	50.5	37.4	30.7	24.7	23.1	19.4	17.2	15.4	13.6
	99.5	33.8	23.3	18.9	16.2	13.2	11.5	10.6	9.1	8.6
	119.4	24.5	17.5	13.7	11.8	9.4	9.0	7.6	6.6	6.5
	139.3	20.6	13.8	11.7	9.4	8.0	7.2	6.4	5.5	4.9
	159.2	15.7	11.9	8.8	7.8	6.5	5.4	5.1	4.5	4.0
	179.1	13.6	9.1	6.9	6.1	5.7	4.7	4.3	4.0	3.8
	199.0	11.1	8.0	6.0	5.7	4.7	4.1	3.6	3.3	3.1
	218.9	10.3	6.5	5.7	4.5	3.9	3.5	3.2	2.9	2.9
	238.8	8.0	6.2	4.3	4.0	4.2	3.3	3.2	2.5	2.5

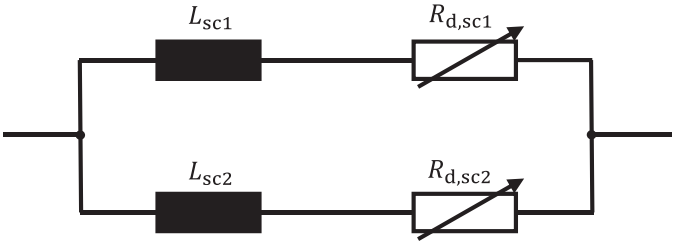

Fig. 11. Electric equivalent circuit of the double-sided triggering experiment shown in Fig. 2.

It can be calculated by (3) and (4) given in [34]

$$L = 2l\left[\log\frac{2l}{R} - 1 + \frac{R}{l}\right] \tag{3}$$

with the length l of the superconductor and the geometric mean distance R

$$R = 0.2235\,(2a + h) \tag{4}$$

where a is the half width of the superconductor and h the thickness of the superconducting layer.

Assuming a straight conductor, the inductance for each superconducting leg is approx. $L_{sc1} = L_{sc2} = 70$ nH. With the dynamic resistance of 5.4 $\mu\Omega$ for a magnetic field of 90 mT and 300 Hz, the time constant of the LR-circuit can be calculated and gives $\tau = 13.1$ ms. This matches well with the measured time. With higher resistances, a faster switching time can be achieved.

V. CONCLUSION AND OUTLOOK

The dynamic resistance is used to investigate the current distribution behavior of parallel HTS tapes. Frequency and magnetic field are varied to investigate the dynamic resistance.

The results of the investigation are as follows.

A dynamic resistance of up to 4.5 mΩ in an active magnetic length of 2 cm could be built up at 1450 Hz and 356.17 mT. The single-sided setup demonstrated the possibility to lower the transport current to zero by generating a dynamic resistance in the superconductor. With zero joint resistance between both parallel paths, the current distribution remains the same after turning the magnet OFF. The double-sided triggering experiment demonstrates fast current switching in parallel HTS paths. The time constant for the current redistribution of 2.5 ms could be achieved whereby this is highly dependent on generated the dynamic resistance.

These experiments show that by utilizing dynamic resistance in HTS superconductors, fully superconducting switching devices are feasible. In general, rectifier circuits in power electronics can be envisaged by upscaling to higher resistances and faster commutation times while still keeping reasonable length of superconductor. These can be used beneficially in high current, low voltage applications, e.g., electrolysis in combination with high current dc superconducting bus bars.

REFERENCES

[1] L. J. M. Van De Klundert and H. H. J. Ten Kate, "Fully superconducting rectifiers and fluxpumps Part 1: Realized methods for pumping flux," *Cryogenics*, vol. 21, no. 4, pp. 195–206, Apr. 1981, doi: 10.1016/0011-2275(81)90195-8.

[2] N. Bykovskiy, A. Dudarev, and H. T. Kate, "Thermally activated ReBCO switches for charging high-current magnets," *IEEE Trans. Appl. Supercond.*, vol. 29, no. 5, Aug. 2019, Art. no. 5502005, doi: 10.1109/TASC.2019.2895849.

[3] S. B. Kim et al., "Current bypassing properties by thermal switch for PCS application on NMR/MRI HTS magnets," *Phys. Procedia*, vol. 65, pp. 149–152, Jan. 2015, doi: 10.1016/j.phpro.2015.05.088.

[4] M. Noe et al., "Conceptual design of a 110 kV resistive superconducting fault current limiter using MCP-BSCCO 2212 bulk material," *IEEE Trans. Appl. Supercond.*, vol. 17, no. 2, pp. 1784–1787, Jun. 2007, doi: 10.1109/TASC.2007.898125.

[5] W. Prusseit, H. Kinder, J. Handke, M. Noe, A. Kudymow, and W. Goldacker, "Switching and quench propagation in coated conductors for fault current limiters," *Phys. C Supercond. Its Appl.*, vol. 445–448, pp. 665–668, Oct. 2006, doi: 10.1016/j.physc.2006.05.014.

[6] A. Kudymow, M. Noe, C. Schacherer, H. Kinder, and W. Prusseit, "Investigation of YBCO coated conductor for application in resistive superconducting fault current limiters," *IEEE Trans. Appl. Supercond.*, vol. 17, no. 2, pp. 3499–3502, Jun. 2007, doi: 10.1109/TASC.2007.899578.

[7] J. Geng and T. A. Coombs, "Mechanism of a high-Tc superconducting flux pump: Using alternating magnetic field to trigger flux flow," *Appl. Phys. Lett.*, vol. 107, no. 14, Oct. 2015, Art. no. 142601, doi: 10.1063/1.4932950.

[8] J. Gawith, J. Geng, J. Ma, B. Shen, C. Li, and T. A. Coombs, "HTS transformer–rectifier flux pump optimization," *IEEE Trans. Appl. Supercond.*, vol. 29, no. 5, Jan. 2019, Art. no. 5501605, doi: 10.1109/TASC.2019.2904444.

[9] J. D. D. Gawith et al., "An HTS power switch using YBCO thin film controlled by AC magnetic field," *Supercond. Sci. Technol.*, vol. 32, no. 9, Jan. 2019, Art. no. 095007, doi: 10.1088/1361-6668/ab2d61.

[10] J. D. D. Gawith et al., "A half-bridge HTS transformer–rectifier flux pump with two AC field-controlled switches," *Supercond. Sci. Technol.*, vol. 31, no. 8, Jan. 2018, Art. no. 085002, doi: 10.1088/1361-6668/aac86d.

[11] J. Geng et al., "HTS persistent current switch controlled by AC magnetic field," *IEEE Trans. Appl. Supercond.*, vol. 26, no. 3, Apr. 2016, Art. no. 6603304, doi: 10.1109/TASC.2016.2540166.

[12] J. Geng et al., "Origin of DC voltage in type II superconducting flux pumps: Field, field rate of change, and current density dependence of resistivity," *J. Phys. Appl. Phys.*, vol. 49, no. 11, Mar. 2016, Art. no. 11LT01, doi: 10.1088/0022-3727/49/11/11LT01.

[13] J. Geng, K. Matsuda, L. Fu, B. Shen, X. Zhang, and T. A. Coombs, "Operational research on a high- T_c rectifier-type superconducting flux pump," *Supercond. Sci. Technol.*, vol. 29, no. 3, Mar. 2016, Art. no. 035015, doi: 10.1088/0953-2048/29/3/035015.

[14] C. W. Bumby, A. E. Pantoja, H.-J. Sung, Z. Jiang, R. Kulkarni, and R. A. Badcock, "Through-wall excitation of a magnet coil by an external-rotor HTS flux pump," *IEEE Trans. Appl. Supercond.*, vol. 26, no. 4, Jun. 2016, Art. no. 0500505, doi: 10.1109/TASC.2016.2526605.

[15] S. Ziegler, R. C. Woodward, H. H.-C. Iu, and L. J. Borle, "Current sensing techniques: A review," *IEEE Sens. J.*, vol. 9, no. 4, pp. 354–376, Apr. 2009, doi: 10.1109/JSEN.2009.2013914.

[16] P. Ripka, "Contactless measurement of electric current using magnetic sensors," *Technisches Messen*, vol. 86, no. 10, pp. 586–598, Oct. 2019, doi: 10.1515/teme-2019-0032.

[17] M. P. Oomen, J. Rieger, M. Leghissa, B. Haken, and H. H. J. Kate, "Dynamic resistance in a slab-like superconductor with Jc (B) dependence," *Supercond. Sci. Technol.*, vol. 12, no. 6, pp. 382–387, Jan. 1999, doi: 10.1088/0953-2048/12/6/309.

[18] H. Zhang, B. Shen, X. Chen, and Z. Jiang, "Dynamic resistance and dynamic loss in a ReBCO superconductor," *Supercond. Sci. Technol.*, vol. 35, no. 11, Nov. 2022, Art. no. 113001, doi: 10.1088/1361-6668/ac95d5.

[19] Z. Jiang, R. Toyomoto, N. Amemiya, X. Zhang, and C. W. Bumby, "Dynamic resistance of a high- Tc coated conductor wire in a perpendicular magnetic field at 77 K," *Supercond. Sci. Technol.*, vol. 30, no. 3, Jan. 2017, Art. no. 0301, doi: 10.1088/1361-6668/aa54e5.

[20] H. Zhang et al., "Modelling of electromagnetic loss in HTS coated conductors over a wide frequency band," *Supercond. Sci. Technol.*, vol. 33, no. 2, Jan. 2020, Art. no. 025004, doi: 10.1088/1361-6668/ab6022.

[21] K. P. Thakur, A. Raj, E. H. Brandt, J. Kvitkovic, and S. V. Pamidi, "Frequency-dependent critical current and transport AC loss of superconductor strip and Roebel cable," *Supercond. Sci. Technol.*, vol. 24, no. 6, Apr. 2011, Art. no. 065024, doi: 10.1088/0953-2048/24/6/065024.

[22] P. Zhou et al., "Frequency-dependent transport AC losses of coated superconductors up to tens of kilohertz," *IEEE Trans. Appl. Supercond.*, vol. 29, no. 5, Aug. 2019, Art. no. 8201705, doi: 10.1109/TASC.2019.2904204.

[23] P. Zhou, G. Ma, and L. Quéval, "Transition frequency of transport AC losses in high temperature superconducting coated conductors," *J. Appl. Phys.*, vol. 126, no. 6, Aug. 2019, Art. no. 063901, doi: 10.1063/1.5094727.

[24] J. Geng et al., "Voltage-ampere characteristics of YBCO coated conductor under inhomogeneous oscillating magnetic field," *Appl. Phys. Lett.*, vol. 108, no. 26, Jun. 2016, Art. no. 262601, doi: 10.1063/1.4955266.

[25] H. Zhang et al., "A full-range formulation for dynamic loss of high-temperature superconductor coated conductors," *Supercond. Sci. Technol.*, vol. 33, no. 5, May 2020, Art. no. 05LT01, doi: 10.1088/1361-6668/ab7b0d.

[26] M. D. Ainslie, C. W. Bumby, Z. Jiang, R. Toyomoto, and N. Amemiya, "Numerical modelling of dynamic resistance in high-temperature superconducting coated-conductor wires," *Supercond. Sci. Technol.*, vol. 31, no. 7, Jul. 2018, Art. no. 074003, doi: 10.1088/1361-6668/aac1d3.

[27] J. Ma, J. Geng, W. K. Chan, J. Schwartz, and T. Coombs, "A temperature-dependent multilayer model for direct current carrying HTS coated-conductors under perpendicular AC magnetic fields," *Supercond. Sci. Technol.*, vol. 33, no. 4, Apr. 2020, Art. no. 045007, doi: 10.1088/1361-6668/ab6fe9.

[28] L. Rostila, J. Lehtonen, and R. Mikkonen, "Self-field reduces critical current density in thick YBCO layers," *Phys. C Supercond.*, vol. 451, no. 1, pp. 66–70, Jan. 2007, doi: 10.1016/j.physc.2006.10.008.

[29] F. Grilli, F. Sirois, V. M. R. Zermeño, and M. Vojenčiak, "Self-consistent modeling of the I_c of HTS devices: How accurate do models really need to be?," *IEEE Trans. Appl. Supercond.*, vol. 24, no. 6, Dec. 2014, Art. no. 8000508, doi: 10.1109/TASC.2014.2326925.

[30] J. Ma et al., "Impact of stabilizer layers on the thermal-electromagnetic characteristics of direct current carrying HTS coated conductors under perpendicular AC magnetic fields," *IEEE Trans. Appl. Supercond.*, vol. 30, no. 4, Jun. 2020, Art. no. 6600906, doi: 10.1109/TASC.2020.2977004.

[31] C. Li, Y. Xing, Y. Xin, B. Li, and F. Grilli, "Time-dependent development of dynamic resistance voltage of superconducting tape considering heat accumulation," *Superconductivity*, vol. 8, Dec. 2023, Art. no. 100066, doi: 10.1016/j.supcon.2023.100066.

[32] H. Merte Jr. and J. A. Clark, "Boiling heat transfer with cryogenic fluids at standard, fractional, and near-zero gravity," *J. Heat Transfer*, vol. 86, no. 3, pp. 351–358, Aug. 1964, doi: 10.1115/1.3688689.

[33] S. Hellmann and M. Noe, "Influence of different surface treatments on the heat flux from solids to liquid nitrogen," *IEEE Trans. Appl. Supercond.*, vol. 24, no. 3, Jun. 2014, Art. no. 0501605, doi: 10.1109/TASC.2013.2283772.

[34] E. B. Rosa, "The self and mutual-inductances of linear conductors," *Bull. Bur. Standards*, vol. 4, no. 2, Jan. 1908, Art. no. 301, doi: 10.6028/bulletin.088.